

**Robustness and Flexibility in Compact Quasiaxial Stellarators: Global
Ideal MHD Stability and Energetic Particle Transport**

M. H. Redi¹, A. Diallo², W. A. Cooper³, G. Y. Fu¹, J. L. Johnson¹,
C. Nührenberg⁴, N. Pomphrey, A. H. Reiman¹, R. B. White¹, M. C. Zarnstorff¹
and the NCSX Team

¹*Princeton Plasma Physics Laboratory, Princeton University, Princeton, NJ 08543*

²*University of Montana, Missoula, MT 59801 USA*

³*CRPP, Lausanne, Switzerland*

⁴*IPP, Greifswald, Germany*

Abstract

Concerns about the flexibility and robustness of a compact quasiaxial stellarator design are addressed by studying the effects of varied pressure and rotational transform profiles on expected performance. For thirty, related, fully three-dimensional configurations the global, ideal magnetohydrodynamic stability is evaluated as well as energetic particle transport. It is found that tokamak intuition is relevant to understanding the magnetohydrodynamic stability, with pressure gradient driving terms and shear stabilization controlling both the periodicity preserving, $N=0$, and the non-periodicity preserving, $N=1$, unstable kink modes. Global kink modes are generated by steeply peaked pressure profiles near the half radius and edge localized kink modes are found for plasmas with steep pressure profiles at the edge as well as with edge rotational transform above 0.5. Energetic particle transport is not strongly dependent on these changes of pressure and current (or rotational transform) profiles, although a weak inverse dependence on pressure peaking through the corresponding Shafranov shift is found. While good transport and MHD stability are not anticorrelated in these equilibria, stability only results from a delicate balance of the pressure and shear stabilization forces. A range of interesting MHD behaviors is found for this large set of equilibria, exhibiting similar particle transport properties.

PACS numbers 52.20.Dq, 52.30.Bt, 52.35.Py, 52.55.Hc, 52.65.-y

I. INTRODUCTION

An intense effort to achieve a stable and well confined compact quasiaxial stellarator (QAS) [1, 2] configuration has led to a promising design for a modest size experiment to be called the National Compact Stellarator Experiment (NCSX) [3, 4]. New ideas for symmetric stellarator design have driven the development of advanced computational tools to evaluate and optimize neoclassical plasma transport and magnetohydrodynamic (MHD) stability in fully three-dimensional geometries. Computational studies can identify conditions which will increase or decrease plasma transport and MHD instability, thereby making possible the design of a stellarator experiment with a range of expected scenarios, to test and improve our understanding of the underlying physics. A plausible picture of the flexibility and robustness of the design configuration can be projected before construction begins.

Loss of plasma confinement has been a historical problem in stellarator experiments, which the new quasisymmetric designs are expected to circumvent. Loss of confinement can be driven by MHD instabilities and by neoclassical and anomalous transport processes. Very recently it has become possible to calculate the probability of these effects for a particular equilibrium, making use of advanced computer packages as well as high performance computing platforms. Although developments in anomalous transport theory are approaching a stage useful for transport predictions, this paper will only investigate predictions for neoclassical transport and ideal MHD stability for one candidate NCSX design, and thirty related equilibria. Such calculations are now a necessary step in the planning of a new experiment.

In Section II we discuss the variations of the pressure and rotational transform profiles considered for equilibria which maintain a fixed boundary shape as well as the average β . The results of the MHD stability and particle transport calculations are given in Sections III and IV. Section V provides a summary and conclusion.

II. THE BASELINE DESIGN AND THE PRESSURE AND ROTATIONAL TRANSFORM VARIATIONS

The baseline case, called QAS3_C82, is the candidate design configuration for NCSX presented at the 1999 EPS meeting [3] and at the 1999 APS meeting [4]. This is a three field period, compact stellarator with major radius 1.6 m, and aspect ratio 3.5. A toroidal field of 1T is assumed at the magnetic axis. To assess flexible performance in a modest-sized experiment, the VMEC code [5] is used to obtain equilibria at $\beta \sim 3.8\%$ for six pressure profiles and five ι profiles, leading to 30 related equilibria exhibiting different stability and transport behaviors. The rotational transform, $\iota = 1/q$, is produced by both external field coils and currents arising from the various sources: the equilibrium-based pressure-dependent bootstrap and Pfirsch-Schlüter currents, in addition to the externally driven ohmic, beam-driven and RF-driven currents. Flux surface cross sections are shown in Figure 1 for the baseline case.

The pressure profiles and ι profiles we consider are shown in Figures 2 and 3. Most stellarator density profiles are broader than the ARIES-like profiles [6] chosen for the initial design for NCSX. The QAS3_C82 current profile was chosen to be similar to that of a bootstrap current profile in a low collisionality reactor, to enable rapid reactor

performance scaling. The plasma equilibria obtained are designated P0X/I0Y as follows: P00/I00 is the baseline QAS3_C82 configuration. P01, P02 and P03 were defined with $P(r) = P_o[\exp(-(s/\sigma)^2) - \exp(-1/\sigma^2)] / (1 - \exp(-1/\sigma^2))$. The edge normalized toroidal flux label s is proportional to $(r/a)^2$ and varies from 0 at the plasma center to 1 at the plasma edge. σ was varied so that P01 is similar to P00, P02 is more peaked than P01, while P03 is broader than P01. For P01, P02 and P03, $\sigma = 0.52, 0.4, 0.7$. P04 is a very broad, parabolic pressure profile defined as $P = P_o (1-s^2)^\alpha$ with $\alpha = 0.5$. P05 is the pressure profile used in the Helias reactor studies based on the W7-X design [7], defined by $P = P_o (1 - 11s/7 + 4s^2/7)$.

The ι profiles are chosen as follows: I01 is linear in s , maintaining the central $\iota(0) = 0.26$ and the edge $\iota(1) = 0.47$, the same as in I00. I04 is also linear in s , with $\iota(a)$ higher than 0.5. We define $\delta = \iota(1) - \iota(0)$, and F as the factor by which the edge shear is increased relative to I01. The ι profiles I01-I04 are written $\iota(s) = \iota(0) + \delta(2-F)s + \delta(F-1)s^2$. The parameters $\iota(0)$, δ and F are shown in Table I.

In this way we can explore the effects of a range of pressure profiles, such as might be generated through on- and off-axis heating and fuelling scenarios, while maintaining the average and edge values of ι similar to those of the baseline case. By studying the equilibria with these pressure profile variations for each ι profile, we look for robust and flexible response from this quasiaxisymmetric stellarator. We can also compare to what would be expected in the axisymmetric, tokamak, case.

III. MAGNETOHYDRODYNAMIC STABILITY

The global, ideal MHD stability of quasiaxial stellarator designs is being evaluated with the three-dimensional stability code packages CAS3D [8-10] and TERPSICHORE [11]. Recently CAS3D has been used to verify and extend calculations [12,13] of the TERPSICHORE code, showing stability of the kink ($N=1$) and periodicity-preserving ($N=0$) modes for the proposed stellarator, even without a conducting wall [14]. The two codes have been extensively benchmarked against tokamak and quasiaxial stellarator equilibria and have been found in good agreement [14]. Most of the stability calculations for the pressure and ι scans of this paper have been obtained with the TERPSICHORE code. The CAS3D code package calculations are found in very good agreement, as is shown below.

TERPSICHORE [11] uses an efficient variational method to solve the equation

$$\delta W_p + \delta W_v - \omega^2 \delta W_k = 0.$$

Here δW_p , δW_v , δW_k and ω^2 represent the potential energy in the plasma, the magnetic energy in the vacuum region, the kinetic energy and the eigenvalue of the system. The MHD perturbations evolve as $\exp(i\omega t)$, being unstable if $\omega^2 < 0$.

Global MHD instability in fully three-dimensional stellarators differs fundamentally from that of axisymmetric tokamaks. The toroidal mode instabilities in tokamaks are not intrinsically coupled [9]. They can be identified by unique toroidal mode numbers $n = 0, \pm 1, \pm 2, \dots$. In stellarators, the toroidal modes are coupled through the magnetic field periodicity. If N_{fp} is the number of field periods of the stellarator, there are $1 + [N_{fp}/2]$ independent mode families for decoupled problems. If $N_{fp} = 3$ as for NCSX, there are two

mode families designated by N . The $N=0$ family, comprising only the coupled toroidal mode numbers $n = 0, \pm 3, \pm 6, \dots$ and the $N=1$ family, comprising only the coupled toroidal mode numbers $n = \pm 1, \pm 2, \pm 4, \pm 5, \dots$. The $N=0$ family is called the even parity or periodicity-preserving mode family while the $N=1$ family is the odd parity mode and is non-periodicity preserving. $N=0$ includes the “vertical” instability ($n=0$) and $N=1$ includes the usual external kink mode ($n=\pm 1$), familiar in tokamak MHD studies. In stellarators, both the $N=0$ and $N=1$ families describe kink-like instabilities.

With an $\iota(r)$ ranging from 0.25 to 0.50 the resonant values of m/n are from 4 to 2. Here m specifies the poloidal mode number. The basis functions for the ideal instabilities are described in mode selection tables, which include m and n for these resonant and nearby m/n values. These tables then comprise the perturbation basis modes assumed for the calculations of the instabilities in the $N=1$ and $N=0$ families. Calculations in this paper use 108 modes and 68 modes, respectively (see Tables II and III). The stability of each equilibrium has been evaluated for the external kink and periodicity-preserving modes for 48, 68 and, in some cases, 96 surfaces. The TERPSICHORE calculations were carried out with a pseudoplasma approximation for the vacuum region, setting the wall distance to 1.5 minor radii away from the plasma boundary.

Figures 4 and 5 summarize the stability of the $N=0$ and $N=1$ modes and how it depends on the pressure and $\iota(r)$ described in the last Section. Configurations were denoted stable on the basis of a) positive eigenvalues for the most unstable mode, or b) if the most unstable mode eigenfunction is a numerical instability, along with convergence studies.

The normal displacements of the unstable eigenfunction ξ and the plasma potential energy change, δW , calculated with TERPSICHORE for the N=0 and N=1 mode families, one for each pressure profile, are shown in Figures 6-10. The figures show the radial shape of the five largest Fourier components of each of the most unstable modes, as well as their identification (m,n).

The CAS3D calculation of ξ and δW for the P02/I00 case, in very good agreement with the TERPSICHORE calculations, is shown in Figure 7. The CAS3D2.vac calculation of the unstable free-boundary perturbation uses the Green's function technique for calculating the vacuum contribution with a conducting wall at infinite distance from the plasma. The calculation is for 128 flux surfaces, uses 108 perturbation harmonics and has the natural resonances eliminated (see discussion below of Figures 12 and 13).

The CAS3D code package [9] solves the same problem as does TERPSICHORE. The calculations are based on the plasma potential energy

$$W_p = 1/2 \iiint d^3r [|\mathbf{C}|^2 - A(\xi \cdot \nabla \mathbf{s})^2 + \gamma p (\nabla \cdot \xi)^2]$$

associated with the displacement ξ . In Figure 7d, C^1 , C^2 and C^3 are components of the vector \mathbf{C} , which stabilizes the plasma energy integral. C^1 describes the field line bending energy, C^2 depends on the local shear and the parallel current density, while C^3 is the field compression energy. δW is the total potential energy change due to the presence of the instability.

Destabilization is driven by the second term in W_p , with the current density \mathbf{j} in A ,

$$A = 2 |\nabla \mathbf{s}|^{-4} (\mathbf{j} \times \nabla \mathbf{s}) \cdot (\mathbf{B} \cdot \nabla) \nabla \mathbf{s}$$

driving instability, modulated by the plasma curvature and the local shear. The third term in W_p is stabilizing. It is proportional to γp , where γ is the ratio of the specific heats and describes the energy associated with field compression. The code version used here is for incompressible modes ($\nabla \cdot \xi = 0$) and therefore the stabilizing term proportional to γp does not contribute.

We find that pressure profile P00 is stable to the kink and the periodicity-preserving modes for all of the ι profiles. P04, on the other hand, is unstable to both modes with all of the ι profiles tested. The P01 and P02 pressure profiles are stable to $N=0$ global modes with all ι profiles. The remaining cases exhibit either stability or instability depending on the ι profile studied. With the very peaked pressure profile, P02, the external kink is unstable for I00, I01 and I02, but is stabilized with I03 and I04. The higher edge ι and increased edge shear of these two ι profiles serve to stabilize the kink for a very peaked pressure profile. The pressure profile characteristic of the Helias reactor studies based on W7-X leads also to a stable external kink for all ι profiles except I04, where the natural resonance at $\iota = 0.5$ is destabilizing. For each pressure profile the unstable modes found were stabilized for ι profiles having increased edge shear, except for the broad “H-mode” pressure profile, P04. Many of the stability calculations at 48 and even 68 flux surfaces exhibited very rapidly varying numerically unstable eigenfunctions with further convergence studies at 96 flux surfaces being necessary.

The VMEC code was used to generate Figure 11, which shows how the parallel current density peaks near the plasma edge and drives the kink unstable for case P04/I00.

The parallel current density is plotted for two configurations which were stable and unstable to the N=0 and N=1 instabilities. Holding ι fixed at the plasma edge leads to this result from the force balance $\nabla\mathbf{P} = \mathbf{j}\times\mathbf{B}$ [15], These instabilities are related to the edge localized modes (ELMS) seen in tokamaks during high heating power H-mode operation. The influence of the edge current density in driving such edge localized modes is well known [16]. The QAS edge localized kink modes (ELKs) are also known in tokamaks as “peeling modes”, and are sometimes precursors to disruptions.

The TERPSICHORE calculations were carried out with a “detuning” factor which smooths the parallel current density profile, at the radial locations with $\iota=3/m$ or $6/m$, *etc.* At these Mercier unstable points for QAS3_C82 (see Fig. 12), the CAS3D calculations show that a locally diverging parallel current density which appears at $\iota=3/7$ ($s= 0.8$) drives kink and vertical instabilities, if resonant contributions are included. This is not found if we assume that an island forms with a locally flattened pressure profile ($\nabla p=0$ in the vicinity of the rational surfaces) or, equivalently, if the natural resonances are eliminated from the calculation. Then the locally diverging parallel current density is suppressed and the corresponding singularities do not appear.

The normal displacements ζ^s of the N=0 and N=1 instabilities are shown in Figure 13 for the case P00/I00 as calculated with CAS3D2.vac without eliminating the natural resonances (Fig.12) and without a locally reduced pressure gradient. The largest Fourier components of the N=1 and N=0 families are shown. The calculations were for free-boundary perturbations for which the vacuum part was computed using the Green’s

function technique with a conducting wall at infinite distance from the plasma. 128 flux surfaces and 68 perturbation harmonics were used for the $N=0$ family, and 108 perturbation harmonics for the $N=1$ family.

An additional set of calculations was carried out to model one possible startup condition, keeping the pressure and ι profiles as in P00/I00, but with β reduced to 1%. This equilibrium is found stable to the $N=0$ and $N=1$ modes.

IV. ENERGETIC PARTICLE TRANSPORT

In recent work with the ORBITMN code [17] we have surveyed a variety of quasiaxial stellarators and examined both thermal and energetic particle transport. It was found that for a three field period, compact stellarator similar to QAS3_C82 (called QAS3_53 (1T) in Ref. 17), a neutral beam of deuterium ions at 40 keV, injected parallel to the magnetic axis, would be depleted in energy by 41% after one slowing down time. We have calculated the effect of the various pressure and ι profiles described above on such a beam of heating ions. Only the pressure and ι dependent changes in the magnetic geometry are included in these simulations, without changes in the deposition profiles or in the slowing down and pitch angle scattering rates. Since peaked pressure profiles lead to more peaked deposition profiles and reduced losses, future work should include these deposition profile effects. Because of the strong q (or ι) dependence in particle transport [18-20] we expect that the ι profile changes would be of primary importance and that there would be little difference in beam ion loss rates among pressure profiles with a fixed ι profile.

Simulations for the complete sequence of equilibria, with deuterium beam ions at 40 keV and a peaked deposition profile, led to similar energetic particle losses in every case (Fig. 14). The P01 pressure profile is based on a Gaussian approximation to the QAS3_C82 pressure profile, leading to slightly increased ion loss rates for these equilibria, 45% after one slowing down time. The figure shows a weak dependence of the particle and energy loss fractions on the position of the magnetic axis and, specifically, the pressure profile dependence. The magnetic axes in these simulations ranged from 1.50 m to 1.63 m, depending on the pressure profile. The statistical error in the particle loss is $\sim (n_{\text{lost}})^{0.5}/n_{\text{total}} \sim \pm 4\%$.

Fig. 15 shows the time evolution of the fraction of beam ion loss in one energy slowing down time for configuration P01/I00. The concave structure of the loss evolution with time is characteristic of QAS [17], and is unlike the convex time evolution plots more typically seen in tokamak beam ion orbit simulations [19, 20]. Over time, more and more ions find their way into loss orbits in the QAS stellarator, while in tokamaks, the incremental losses decrease with time. High initial losses from the parallel beam occur because of banana width and “orbit wobble” and are also not found in tokamaks.

To investigate the stellarator energetic particle loss characteristics, we launched an ensemble of 4000 neutral beam ions in the baseline configuration, with random initial pitch and without any pitch angle scattering. Figure 16 shows the time dependence of the lost beam ions. Regions of highest particle density represent locations in energy/pitch space characterised by high particle loss. In an axisymmetric tokamak these collisionless losses would occur very rapidly, and entirely during the first toroidal orbit. However, in the QAS a

spectrum of longer time scales are observed for the collisionless beam ion loss. It is interesting to note the pocket of high beam ion losses ($0.6 < \lambda < 0.8$ for pitch = $\lambda = v_{//}/v$) due to the collisionless stochastic loss of passing beam ions. This phenomenon has been termed “bucket transport” by Mynick [21,22] and arises for energetic ions after some energy slowing down has occurred. Simulations of alpha loss from TFTR which were compared to pellet charge exchange measurements of the confined alpha particle distribution, also showed small losses attributed to stochastic collisionless passing alpha particles [23], resulting from toroidal field ripple.

For the most part these results confirm our expectations; there is little effect on energetic particle transport from the variations in plasma pressure and ι . The P03 cases with the magnetic axis at 1.5 m, exhibit somewhat reduced energetic particle loss, as ions near the axis are less likely to intersect the last closed flux surface. The I04 cases all have somewhat higher edge ι but this was not sufficient to greatly lower particle losses. We note that the particle transport is only slightly greater in regions of MHD stability and slightly lower in regions of N=0 mode instability. The N=1 unstable cases P02/I00, P02/I01 and P02/I02 did not exhibit clearly reduced particle transport, compared to the kink stable cases P02/I03 and P02/I04. A case of reduced plasma β (1%) with P00/I00, which was chosen to model startup, has a small magnetic axis shift and reduced levels of neutral beam ion energy transport (37%). The thirty equilibria showing a range of MHD behaviors, are not characterized by greatly different particle transport properties.

V. CONCLUSIONS

A series of simulations and calculations varying the pressure and ι profiles for a compact quasiaxial stellarator has shown that the stability of the $N=1$ and $N=0$ families of global ideal MHD is quite dependent on the particular pressure and ι profiles chosen. Calculations for fixed edge poloidal flux and fixed plasma boundary shape at 3.8% beta show that many of the concepts in tokamak MHD are useful in understanding how instabilities arise in QAS.

The calculations show quantitatively how these changes in the plasma configuration affect the global ideal MHD stability and energetic particle transport. Unlike early configurations studied before finding the candidate configuration, in which variations in plasma boundary shape and ι profiles led to either improved kink stability or improved particle transport, but not both; in this study good particle confinement is not anticorrelated with MHD stability. The variables which affected stability most strongly are the plasma pressure gradient which is destabilizing, and the edge shear and edge ι below 0.5, which were stabilizing. The parameters which most strongly affected the energetic particle transport are the Shafranov shift of the magnetic axis and the plasma ι ; low shift and high ι being correlated with better energetic particle confinement.

Global and edge localized kink modes are found to be generated by pressure profiles peaked near the half radius and the plasma edge, respectively, although increased shear can provide some stabilization. Unstable edge localized modes are found for most plasmas with edge ι above 0.5. In tokamaks, edge current density (which drives the ELKS in the QAS

simulations here and ELMS in tokamak H-modes) is found to stabilize global kink modes. Similarly the QAS cases with high edge pressure gradients and high edge current density displayed ELKS, but not global kink modes.

Energetic particle transport is not strongly dependent on these changes of pressure and τ profiles, although a weak inverse dependence on pressure peaking through the resulting Shafranov shift is found. We have recently shown that in QAS the thermal and energetic particle transport behavior are correlated [17], so that we expect these plasmas will also not differ greatly in their thermal ion confinement. While good transport and MHD stability are not anticorrelated in these thirty equilibria, stability only results from a delicate balance of the pressure and shear stabilization forces. Although the baseline design has been shown to be robustly stable relative to the tokamak vertical instability [13], we have shown in Section III that variations in the pressure and τ profiles can lead to “vertical” ($N=0$ kink mode) instability, if the boundary and β are kept constant. It is important to note that this “vertical”, $N=0$, instability arises only for plasmas which are also kink ($N=1$) mode unstable.

A range of interesting MHD behaviors have been found for a large set of equilibria with not dissimilar particle transport properties. The particular pressure and τ profiles used can be considered as targets for experimental planning to develop effective methods for plasma fuelling, heating, current drive and for coil design. The construction of such a device will provide an opportunity for interesting and flexible plasma physics experiments against which modern computational plasma theory can be tested.

Acknowledgements

We are glad to thank G. H. Neilson, R. J. Hawryluk and R. J. Goldston, Princeton Plasma Physics Laboratory, for their encouragement and support. We gratefully acknowledge S. Hirshman, Oak Ridge National Laboratory, for use of the VMEC code and L.-P. Ku, S. Ethier and D. McCune, Princeton Plasma Physics Laboratory, for computational support. A. Diallo was supported at the Princeton Plasma Physics Laboratory during the summer of 1999 through the Department of Energy National Undergraduate Fellowship Program.

*Supported by the US Dept. of Energy Contract DE-AC02-76CH03073.

References

- [1] J. Nührenberg, W. Lotz and S. Gori, in *Theory of Fusion Plasmas*, E. Sindoni, F. Troyon and J. Vaclavik eds., SIF, Bologna, 3 (1994).
- [2] P. Garabedian, *Phys. Plas.* **3**, 2483 (1996).
- [3] A. H. Reiman, G. Fu, S. Hirshman, L. Ku, D. Monticello, H. Mynick, *et al.*, “Physics Design of a High Beta Quasi-axisymmetric Stellarator”, EPS, 1999, Maastricht, Netherlands, paper TL18.
- [4] G. H. Neilson, A. H. Reiman, M. C. Zarnstorff, A. Brooks, G-Y. Fu, *et al.*, “Physics Basis for High-Beta, Low-Aspect-Ratio Stellarator Experiments”, in preparation (1999).
- [5] S. P. Hirshman, W. I. Van Rij, and P Merkel, *Comput. Phys. Commun.* **43**, 143 (1986).
- [6] S. Jardin, C. Kessel, C. Bathke, D. Ehst, T. Mau, F. Najmabadi, T. Petrie, *Fusion Engineering and Design*, **38**, 27 (1997).
- [7] E. Strumberger, H. Wobig, J. Kisslinger, C. Nührenberg, “Equilibrium and Stability Properties of a Helias Reactor”, EPS, 1999, Maastricht, Netherlands, paper P4.031. IPP-Report (1999) IPP 38249.
- [8] C. Nührenberg, *Phys. Plas.* **3**, 2401 (1996).
- [9] C. Schwab, *Phys.Fluids B* **5**, 3195 (1993).
- [10] C. Nührenberg, *Phys. Plas.* **6**, 137 (1999).
- [11] W. A. Cooper, D. B. Singleton, R. L. Dewar, *Phys. Plas.* **3**, 275 (1996).
- [12] G. Y. Fu, L.-P. Ku, N. Pomphrey, M. H. Redi, *et al.*, IAEA-CN-69/THP1/07, 17th IAEA Fusion Energy Conf., Yokahama, 1998.

- [13] G. Y. Fu, L. P. Ku, W. A. Cooper, S. H. Hirshman, D. A. Monticello, *et al.*, “MHD Stability in Compact Stellarators”, submitted to *Phys. Plas.*, 1999.
- [14] M. H. Redi, C. Nührenberg, W. A. Cooper, G.-Y. Fu, C. Kessel, *et al.*, “Vertical and Kink Mode Stability Calculations for Current Carrying Quasiaxial Stellarators”, EPS, 1999, Maastricht, Netherlands, paper P4.085.
- [15] C. E. Kessel, *Nucl. Fusion* **34**, 1221 (1994).
- [16] J. Manickam, *Phys. Fluids* **B4**, 1901 (1992).
- [17] M. H. Redi, H. E. Mynick, M. Suewattana, R. B. White, M. C. Zarnstorff, *Phys. Plas.*, **6**, 3509 (1999).
- [18] R. J. Goldston, R. B. White, A. H. Boozer, *Phys. Rev. Lett.* **47**, 647 (1981).
- [19] M. H. Redi, R. V. Budny, D. S. Darrow, H. H. Duong, R. K. Fisher, *et al.*, *Nucl. Fusion* **35**, 1509 (1995).
- [20] M. H. Redi, M. C. Zarnstorff, R. B. White, R. V. Budny, A. C. Janos *et al.*, *Nucl. Fusion* **35**, 1191 (1995).
- [21] H. Mynick, *Phys. Plas.* **B5**, 1471 (1993).
- [22] H. Mynick, *Phys. Plas.* **5**, 2460 (1993).
- [23] M. H. Redi, S. H. Batha, R. V. Budny, D. S. Darrow, F. M. Levinton *et al.*, *Phys. Plas.* **6**, 2826 (1999).

Table I Parameters of rotational transform profiles , $\iota(s) = \iota(0) + \delta(2-F)s + \delta(F-1)s^2$.

Profile	$\iota(0)$	δ	F
I01	0.26	0.21	1.0
I02	0.26	0.21	1.5
I03	0.26	0.21	2.0
I04	0.26	0.26	1.0

Table II Basis functions (68 modes) used for calculations of the N=0 family most unstable eigenfunctions.

m =	0	1	2	3	4	5	6	7	8	9	10	11	12	13
n														
-4	0	0	0	0	0	0	0	0	0	0	0	0	0	0
-3	0	1	1	1	1	1	1	1	1	1	1	1	1	1
-2	0	0	0	0	0	0	0	0	0	0	0	0	0	0
-1	0	0	0	0	0	0	0	0	0	0	0	0	0	0
0	0	1	1	1	1	1	1	1	1	1	1	1	1	1
1	0	0	0	0	0	0	0	0	0	0	0	0	0	0
2	0	0	0	0	0	0	0	0	0	0	0	0	0	0
3	1	1	1	1	1	1	1	1	1	1	1	1	1	1
4	0	0	0	0	0	0	0	0	0	0	0	0	0	0
5	0	0	0	0	0	0	0	0	0	0	0	0	0	0
6	1	1	1	1	1	1	1	1	1	1	1	1	1	1
7	0	0	0	0	0	0	0	0	0	0	0	0	0	0
8	0	0	0	0	0	0	0	0	0	0	0	0	0	0
9	1	1	1	1	1	1	1	1	1	1	1	1	1	1
10	0	0	0	0	0	0	0	0	0	0	0	0	0	0

Table III Basis functions (108 modes) used for calculations of the N=1 family most unstable eigenfunctions.

m =	0	1	2	3	4	5	6	7	8	9	10	11	12	13
n														
-8	0	0	0	0	0	0	0	0	0	0	0	0	0	0
-7	0	0	0	0	0	0	0	0	0	0	0	0	0	0
-6	0	0	0	0	0	0	0	0	0	0	0	0	0	0
-5	0	1	1	1	1	1	1	1	1	1	1	1	1	1
-4	0	1	1	1	1	1	1	1	1	1	1	1	1	1
-3	0	0	0	0	0	0	0	0	0	0	0	0	0	0
-2	0	1	1	1	1	1	1	1	1	1	1	1	1	1
-1	0	1	1	1	1	1	1	1	1	1	1	1	1	1
0	0	0	0	0	0	0	0	0	0	0	0	0	0	0
1	1	1	1	1	1	1	1	1	1	1	1	1	1	1
2	1	1	1	1	1	1	1	1	1	1	1	1	1	1
3	0	0	0	0	0	0	0	0	0	0	0	0	0	0
4	1	1	1	1	1	1	1	1	1	1	1	1	1	1
5	1	1	1	1	1	1	1	1	1	1	1	1	1	1
6	0	0	0	0	0	0	0	0	0	0	0	0	0	0

Figure Captions

Figure 1. Flux surface cross sections of QAS3_C82 at toroidal angle $\phi = 0^\circ, 90^\circ, 180^\circ$ and 270° within each field period.

Figure 2. Pressure profiles studied for their effect on stability and transport. The flux label s is the edge normalized toroidal flux, and is proportional to $(r/a)^2$.

Figure 3. τ profiles studied for their effect on stability and transport. The flux label s is the edge normalized toroidal flux.

Figure 4. Stability diagram for N=1 mode family for thirty equilibrium configurations.

Figure 5. Stability diagram for N=0 mode family for thirty equilibrium configurations.

Figure 6. TERPSICHORE calculation of the unstable kink mode for P01/I04. The largest Fourier components are (2,1), (4,2), (8,4), (3,1), and (10,5). The flux label s is the edge normalized toroidal flux.

Figure 7. TERPSICHORE and CAS3D calculations of the unstable external kink mode for P02/I00. This is the odd parity perturbation, calculated for 128 flux surfaces, 108 harmonics and the N=1 family. The flux label s is the edge normalized toroidal flux.

Figure 7a: The largest Fourier components of the normal displacement ξ from the TERPSICHORE calculation are (3,1), (4,1), (5,2), (6,2), and (5,1).

Figure 7b: TERPSICHORE calculation of the flux surface averaged energy associated with the normal displacement shown in Fig. 7a.

Figure 7c: The largest Fourier components of the normal displacement ξ from the CAS3D calculation are (3,-1), (4,-1), (6,-2), (5,-2), and (5,-1). The two code packages use different

conventions in the Fourier series. CAS3D defines $f(s,\theta,\phi) = \sum_{m,n} f_{mn} \cos [2\pi(m\theta + n\phi)]$, while TERPSICHORE defines $f(s,\theta,\phi) = \sum_{m,n} f_{mn} \cos [2\pi(m\theta - n\phi)]$,

Figure 7d: CAS3D calculation of the components of the flux surface averaged energy, δW , associated with the normal displacement shown in Fig. 7c.

Figure 8. TERPSICHORE calculation of the unstable kink and periodicity conserving modes for P03/I04. The largest Fourier components of the N=1 family are (4,2), (2,1), (10,5), (5,2), and (8,4). The largest Fourier components of the N=0 family are (6,3), (12,6), (7,3), (11,6), and (5,3). The flux label s is the edge normalized toroidal flux.

Figure 9. TERPSICHORE calculation of the unstable kink and periodicity-conserving modes for P04/I02. The largest Fourier components of the N=1 family are (9,4), (2,1), (11,5), (3,1), and (8,4). The largest Fourier components of the N=0 family are (7,3), (6,3), (13,6), (8,3), and (12,6). The flux label s is the edge normalized toroidal flux.

Figure 10. TERPSICHORE calculation of the unstable kink and periodicity conserving modes for P05/I04. The largest Fourier components of the N=1 family are (4,2), (2,1), (10,5), (8,4), and (5,2). The largest Fourier components of the N=0 family are (6,3), (12,6), (7,3), (11,6), and (5,3). The flux label s is the edge normalized toroidal flux.

Figure 11. Parallel current, $(\mathbf{j} \cdot \mathbf{B}) / \langle \nabla \phi \cdot \mathbf{B} \rangle$, for an ideal MHD unstable case and for a stable case, as calculated with VMEC. Only the nonresonant part of $\mathbf{j} \cdot \mathbf{B}$ is included.

Figure 12. Mercier instability criterion for configuration P00/I00. The resonant part of $\mathbf{j} \cdot \mathbf{B}$ has been accounted for, giving the Mercier resonances identified by D_I . The profiles of the plasma pressure and τ are shown.

Figure 13. CAS3D predictions of the largest Fourier components of the most unstable modes for the N=0 and N=1 instability in configuration P00/I00. In these calculations the natural resonances have not been eliminated. Identification of the 10 largest Fourier component harmonics is shown. These modes are stabilized if the natural resonances are eliminated.

Figure 14. Particle and energy loss percentages for thirty equilibrium configurations. A unique symbol for each pressure profile, P0X, is used to designate the particle loss fractions as shown near the bottom of the figure. The five different equilibrium configurations found with five τ profiles for each P0X, lead to five different, but similar values for the position of the magnetic axis. The energy losses are not differentiated by symbols for each P0X, but can be identified by the major radius location for each configuration and the symbol marking the corresponding particle loss percentage.

Figure 15. Time evolution of beam ion loss from P01/I00 during one slowing down time.

Figure 16. Time of loss for neutral beam ions in P00/I00 orbiting without pitch angle scattering shown as a function of initial pitch angle. Initial ensemble of 4000 ions had random initial pitches.

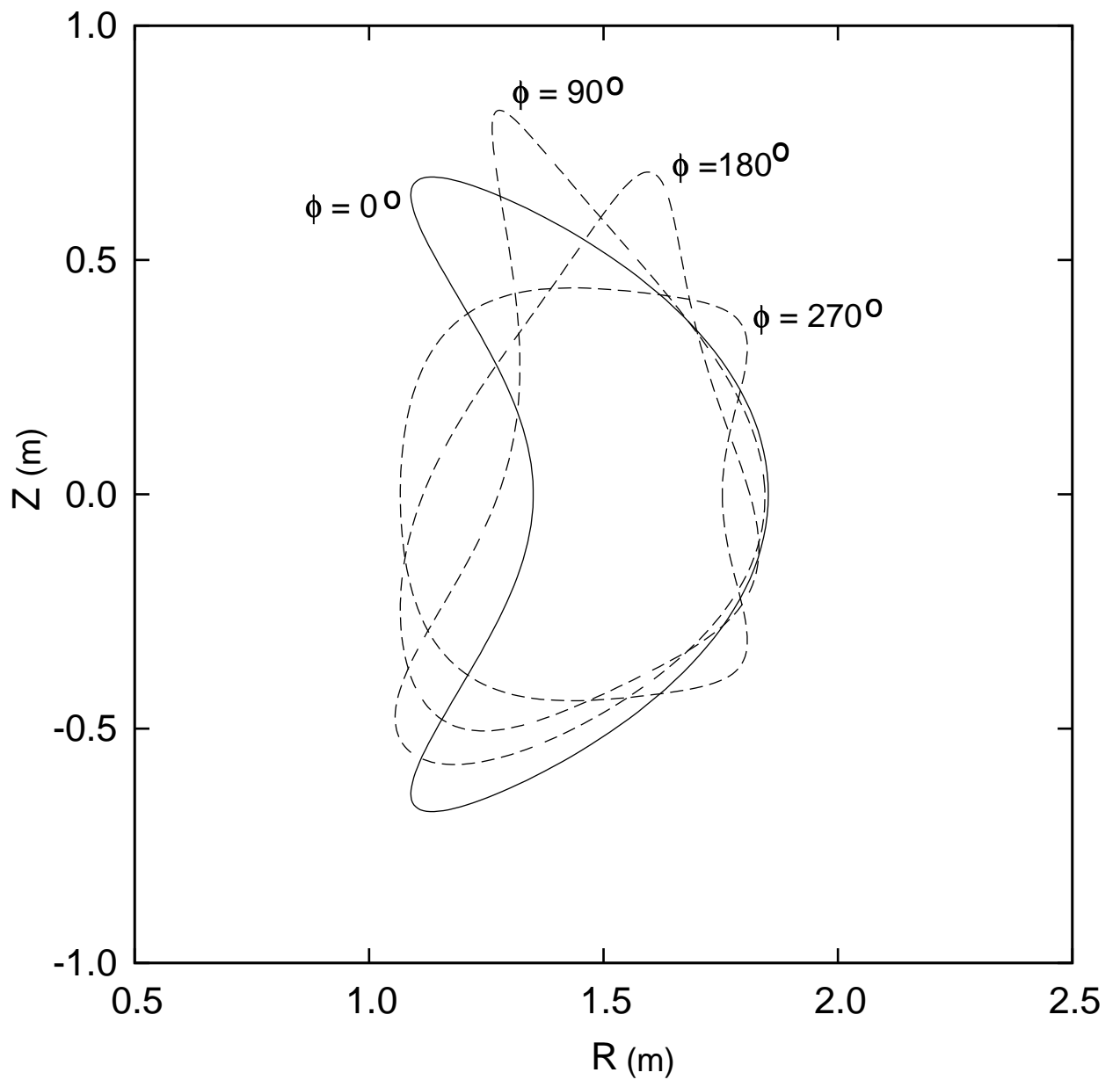


Figure 1

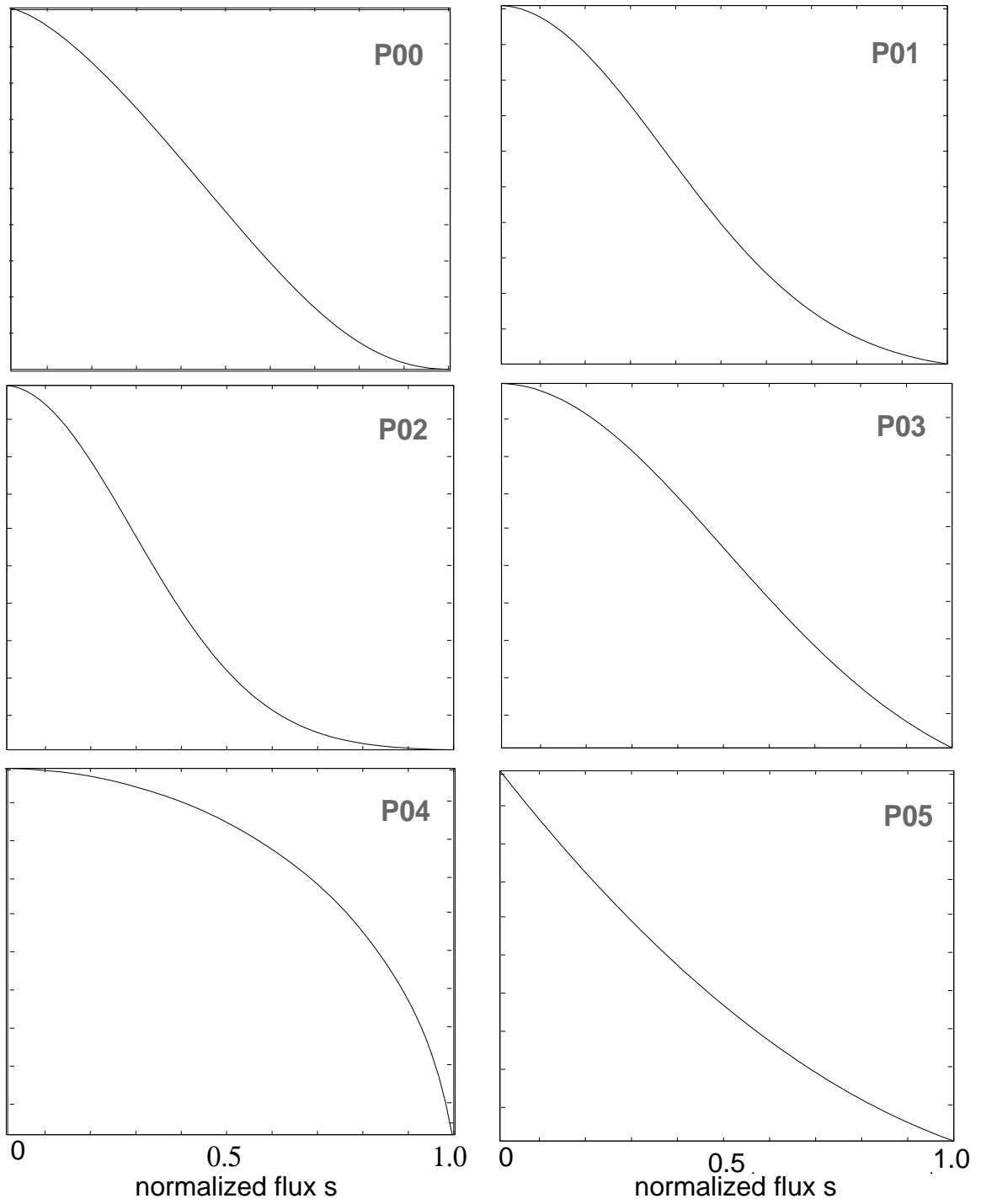


Figure 2

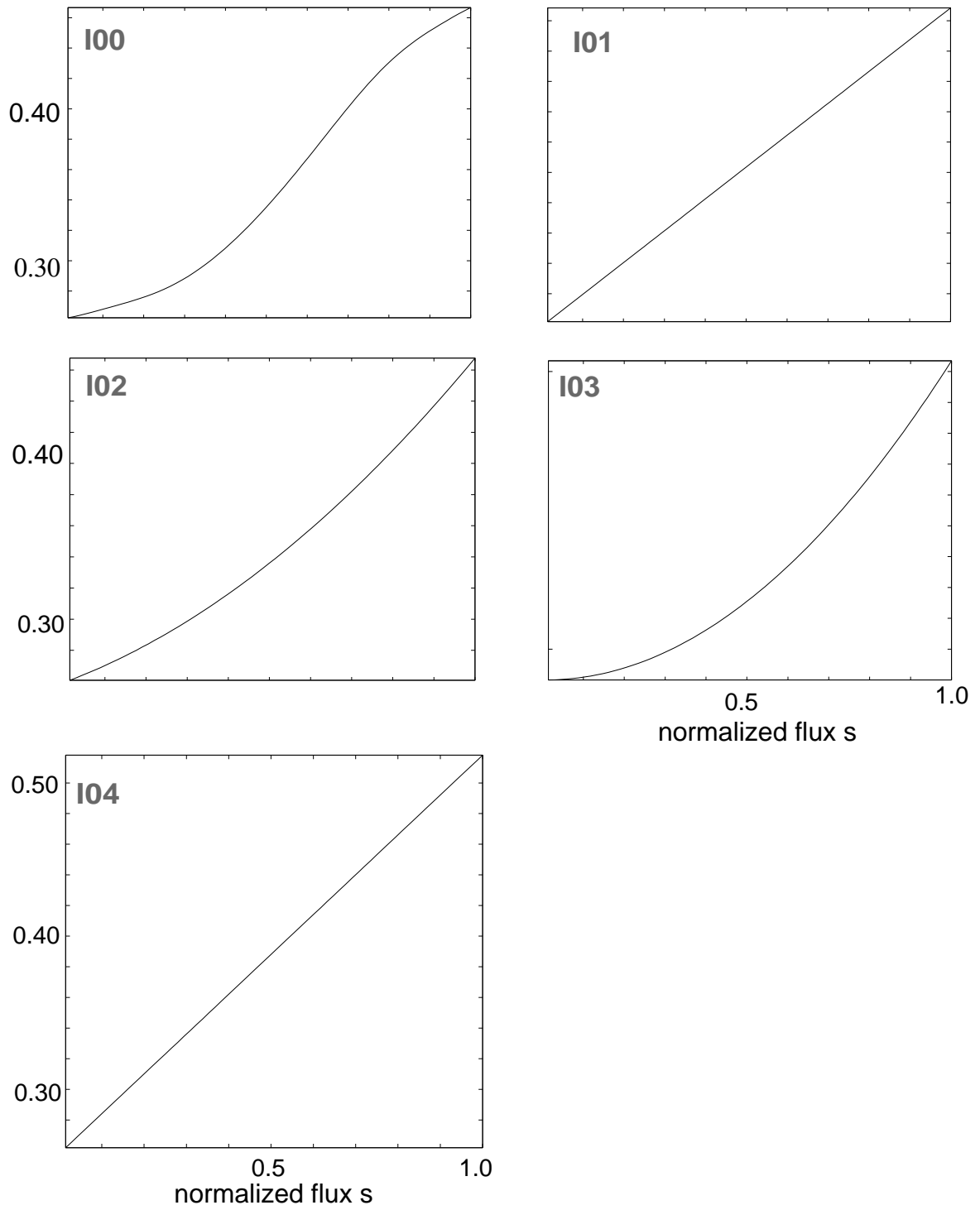


Figure 3

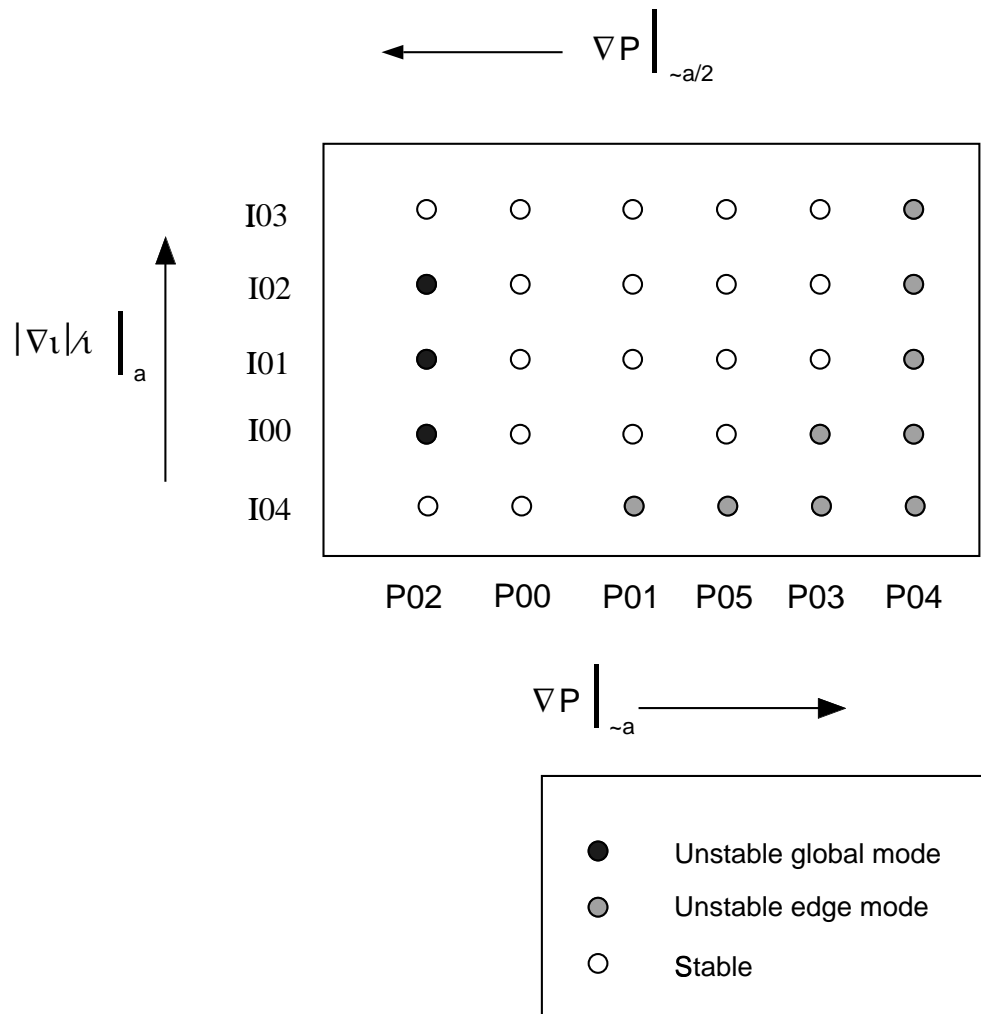


Figure 4

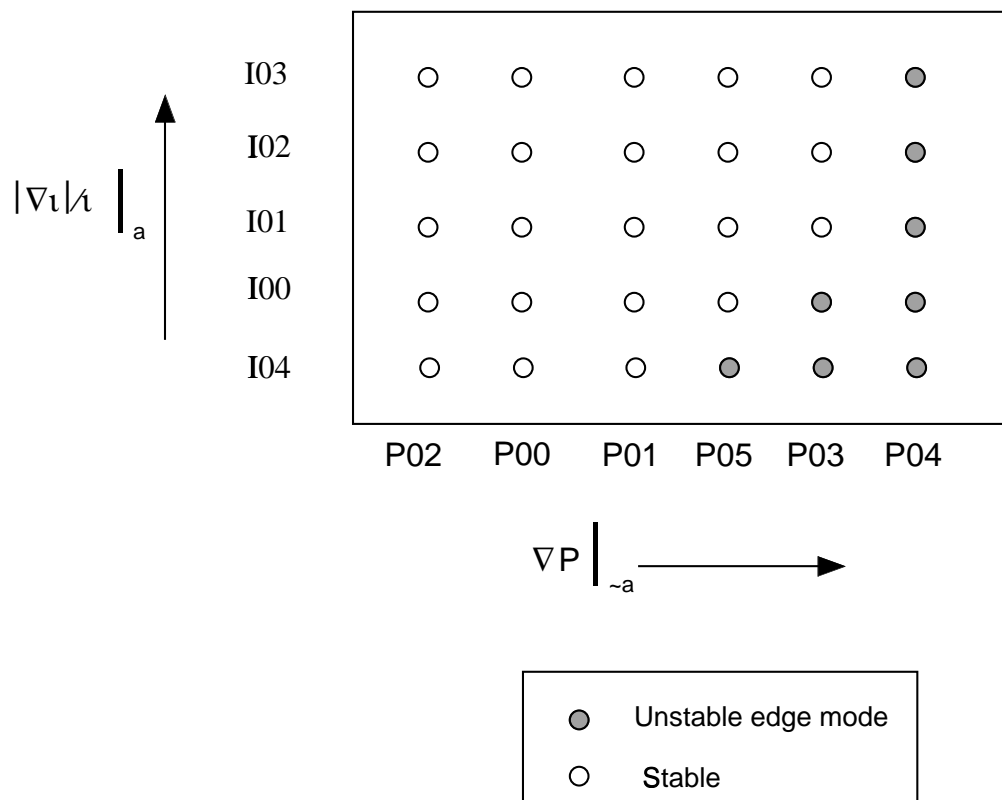


Figure 5

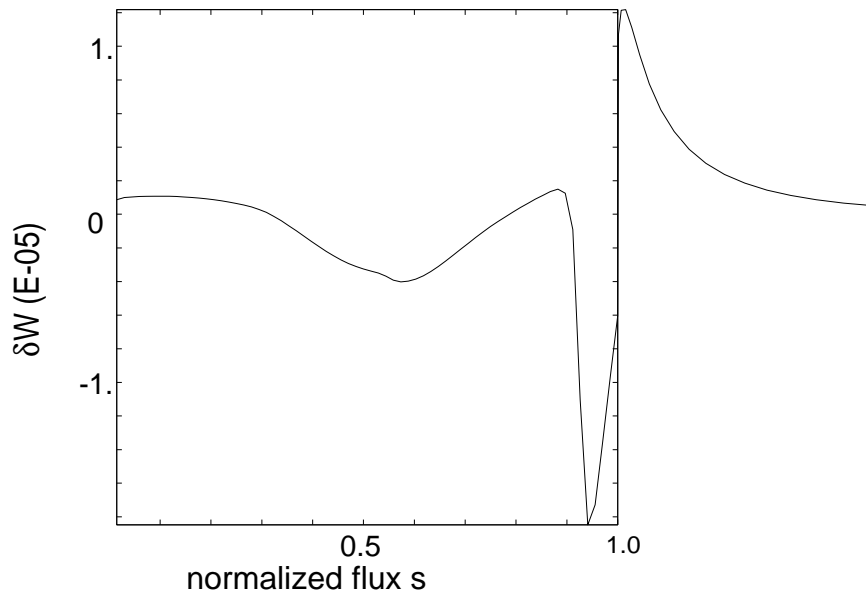
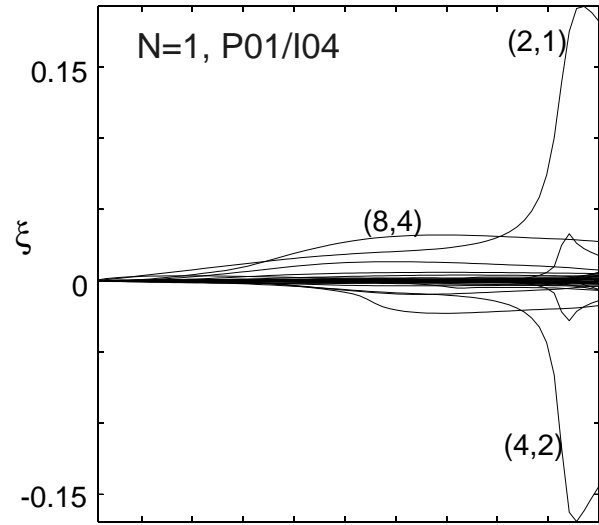


Figure 6

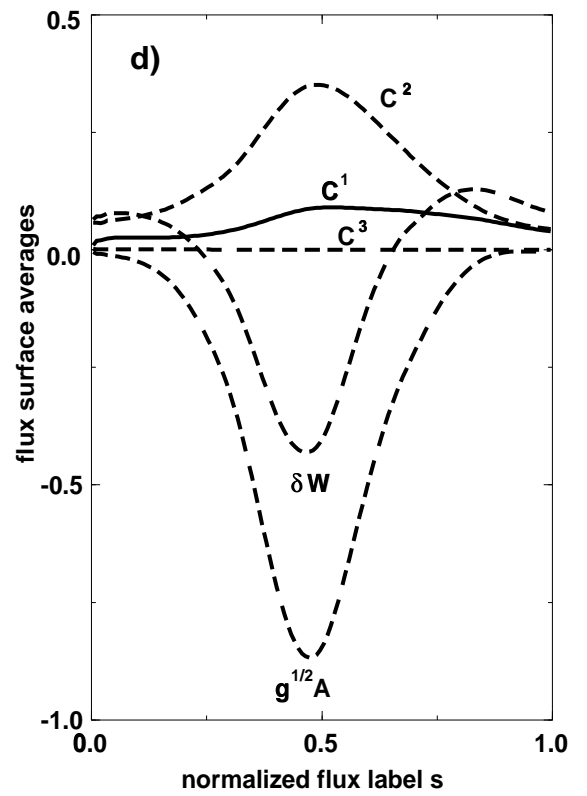
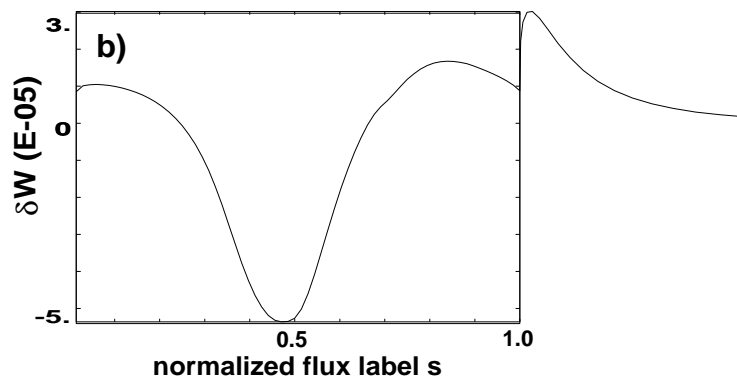
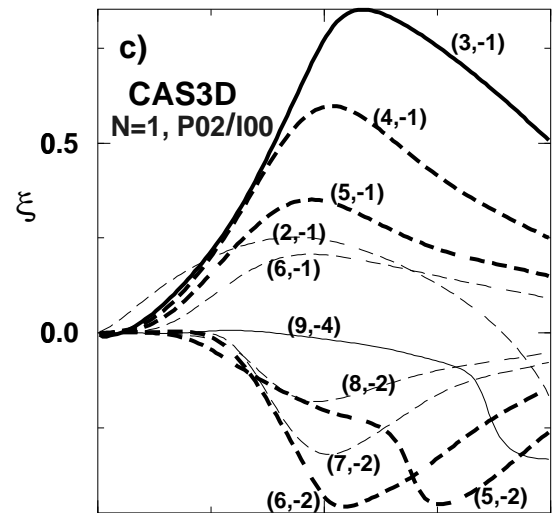
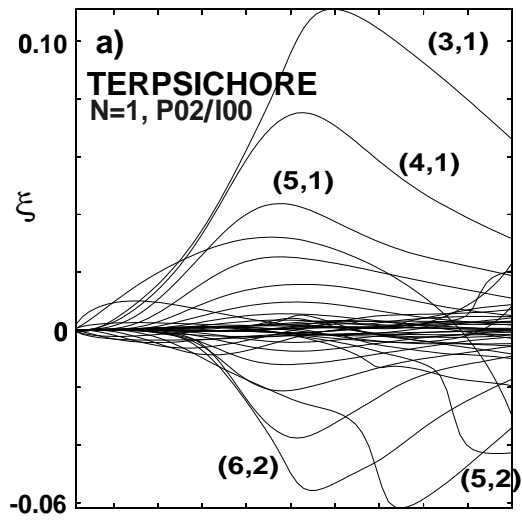


Figure 7

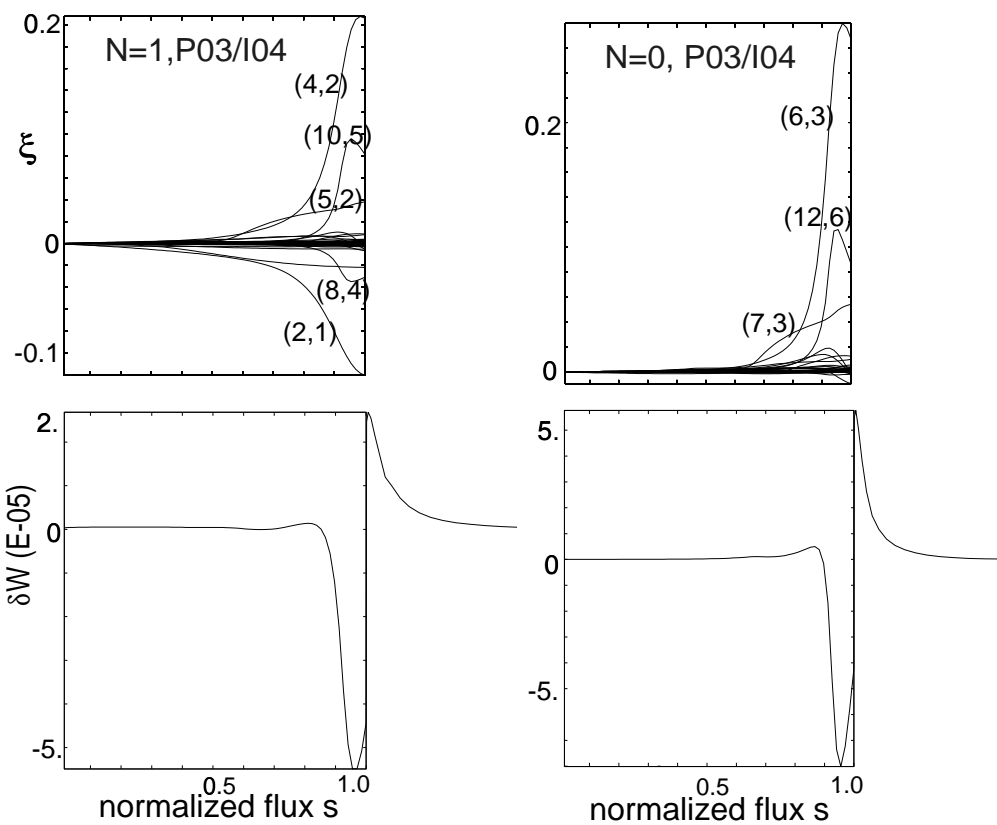


Figure 8

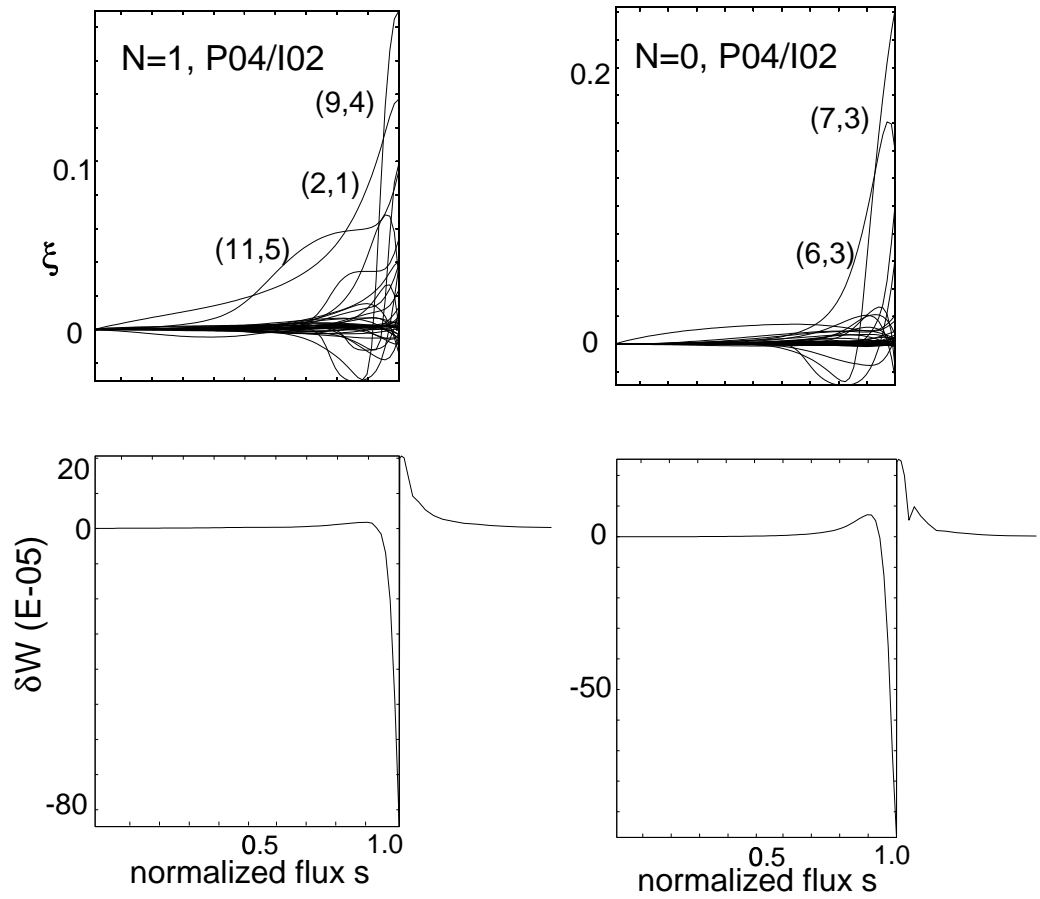


Figure 9

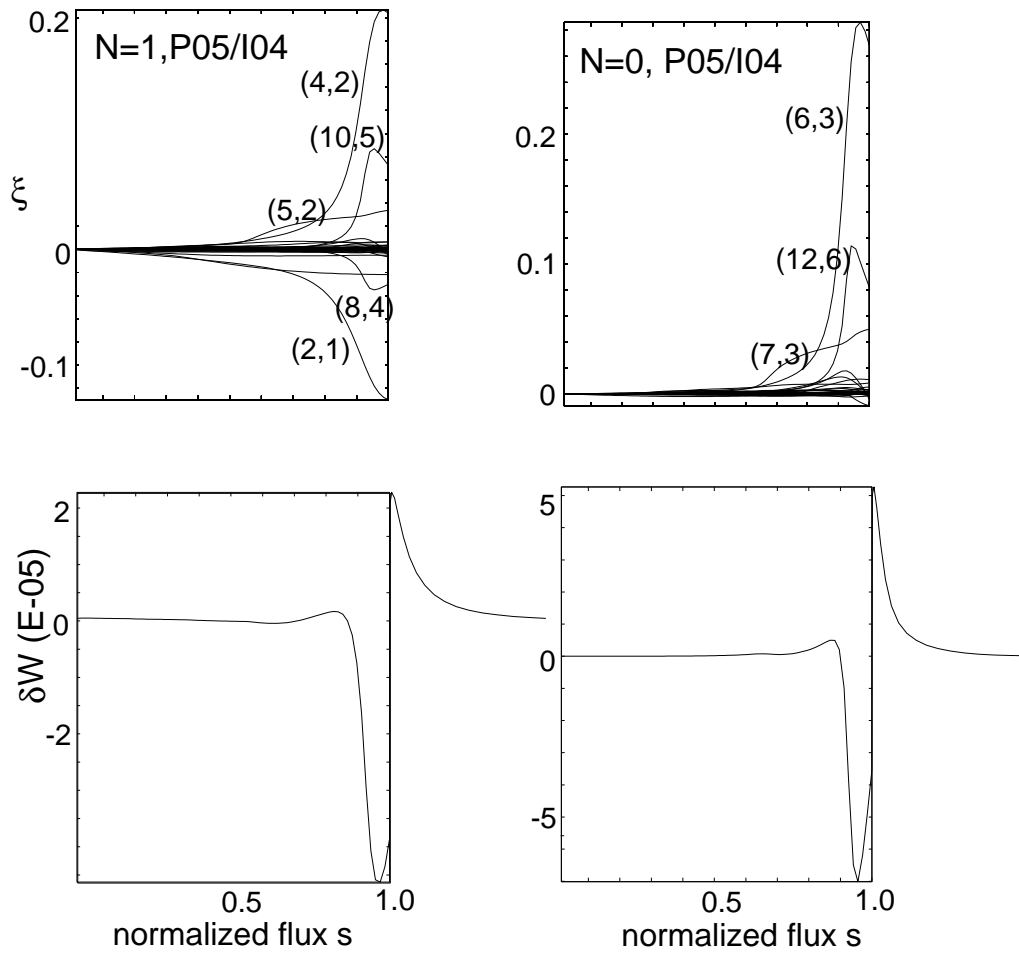


Figure 10

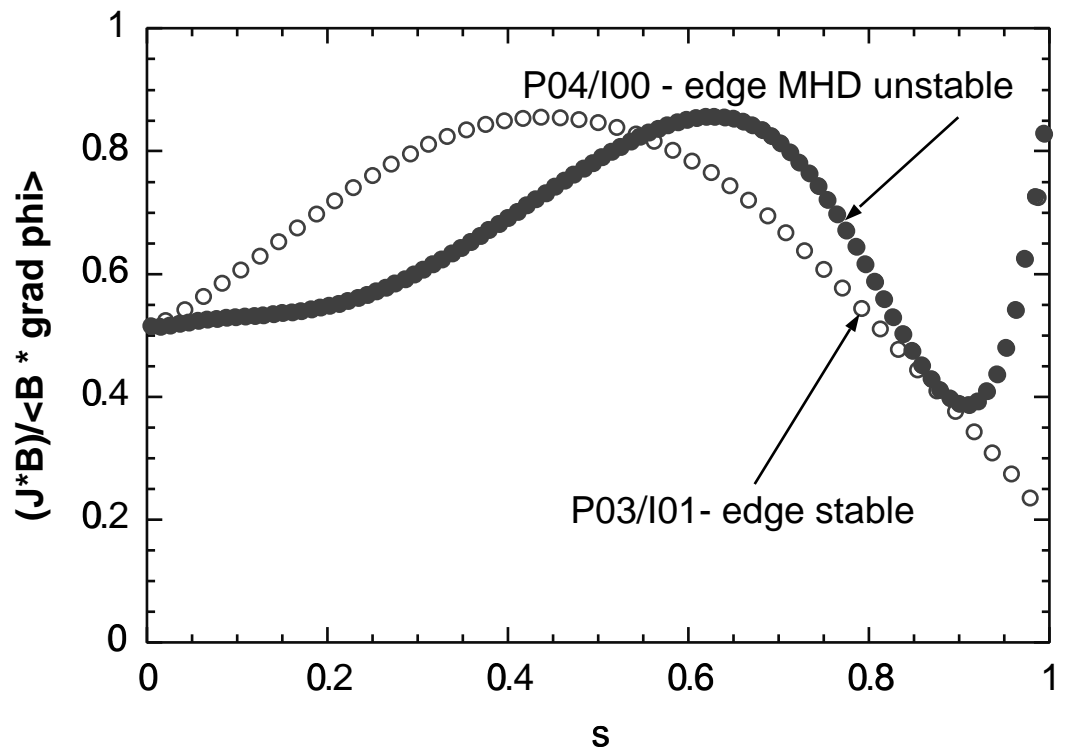


Figure 11

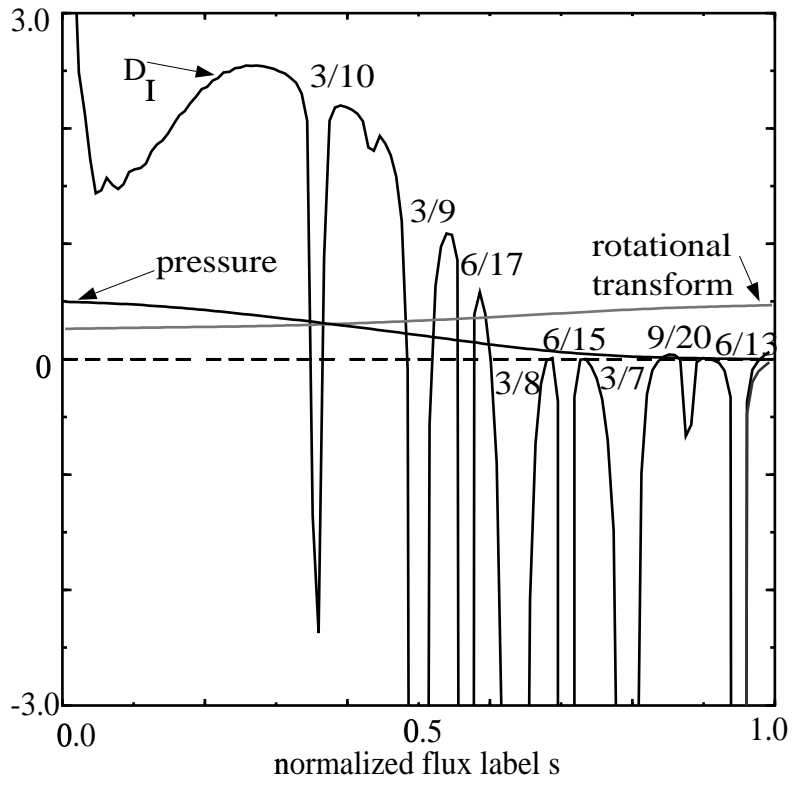


Figure 12

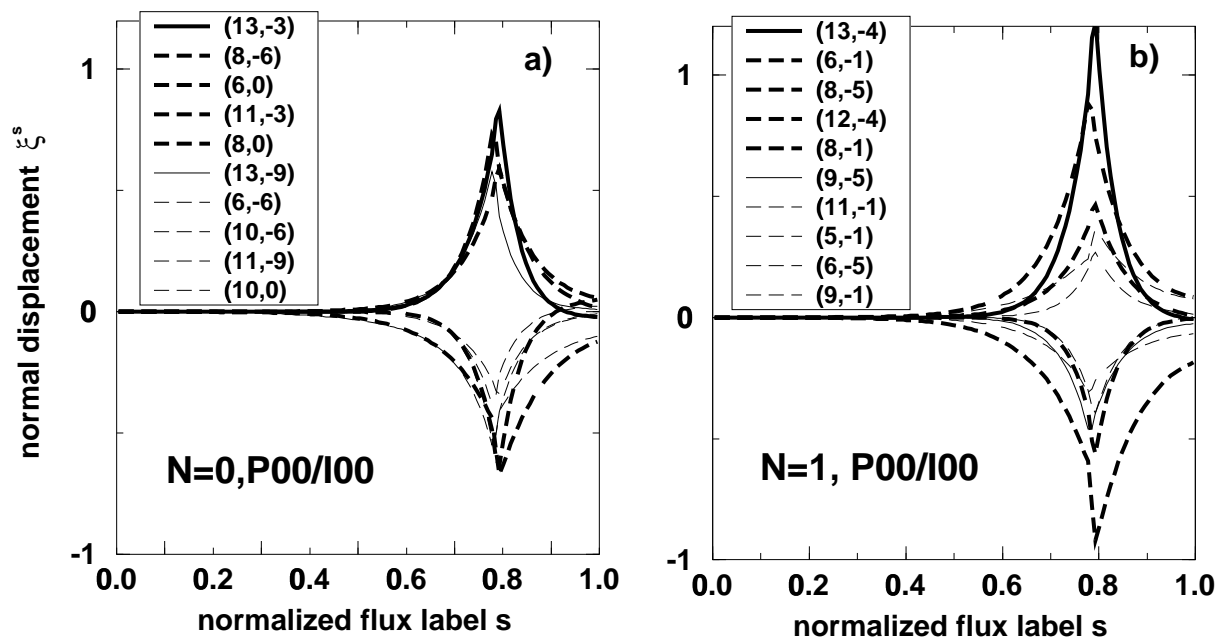


Figure 13

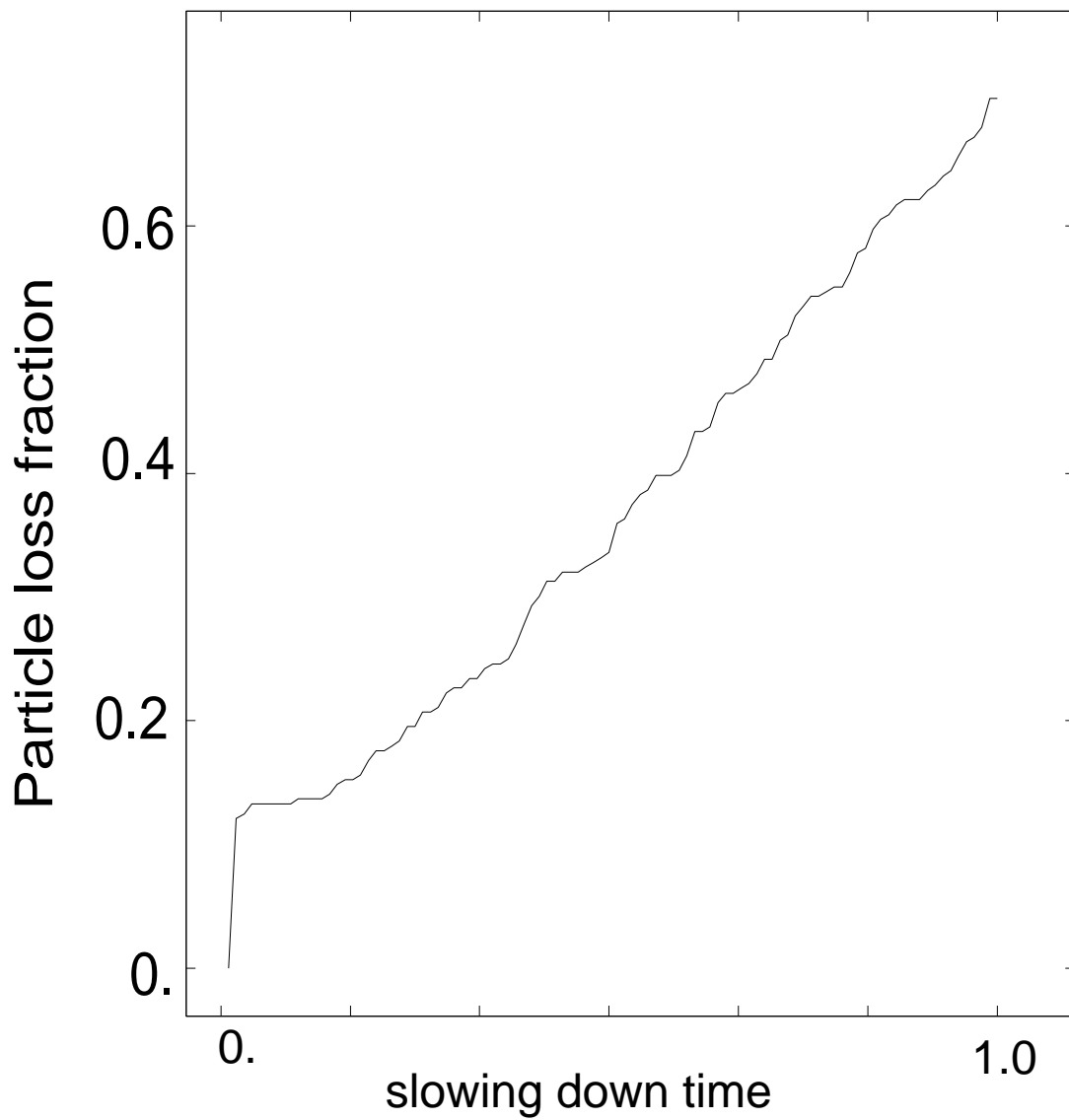


Fig. 15

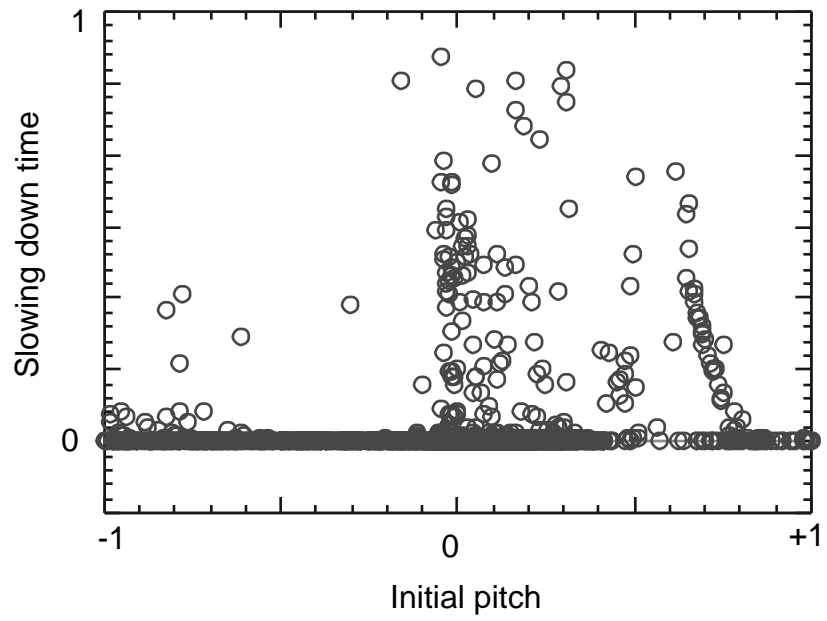


Figure 16